Modelling and Simulation in
Materials Science and Engineering

PAPER • OPEN ACCESS

Polycrystalline silicon, a molecular dynamics study: I. Deposition and growth modes

To cite this article: Mikael Santonen *et al* 2024 *Modelling Simul. Mater. Sci. Eng.* **32** 065025

View the article online for updates and enhancements.

You may also like

- Gettering in Large-Grained Thin Polycrystalline Silicon Films on Glass Substrate
Akito Hara and Tsutomu Sato
- Electrical Properties of Polycrystalline $Si_{1-x}Ge_x$ Thin-Films Prepared by a Solid-Phase Crystallization Method
Yoichiro Aya, Katsutoshi Takeda, Kenichiro Wakisaka et al.
- Characterization and Reliability of Gate-All-Around Poly-Si TFTs with Multinanowire Channels
Han-Wen Liu, Si-Ming Chiou, Chung-En Hung et al.

This content was downloaded from IP address 130.232.39.44 on 14/08/2024 at 06:41

OPEN ACCESS
IOP Publishing
Modelling and Simulation in Materials Science and Engineering
Modelling Simul. Mater. Sci. Eng. **32** (2024) 065025 (21pp)
https://doi.org/10.1088/1361-651X/ad5dd2

Polycrystalline silicon, a molecular dynamics study: I. Deposition and growth modes

Mikael Santonen[1], Antti Lahti[1,*], Zahra Jahanshah Rad[1], Mikko Miettinen[1], Masoud Ebrahimzadeh[1], Juha-Pekka Lehtiö[1], Pekka Laukkanen[1], Marko Punkkinen[1], Petriina Paturi[1], Kalevi Kokko[1], Antti Kuronen[2], Wei Li[3], Levente Vitos[3,4], Katja Parkkinen[5] and Markus Eklund[5]

[1] Department of Physics and Astronomy, University of Turku, FI-20014 Turku, Finland
[2] Department of Physics, University of Helsinki, PO Box 43, FI-00014 Helsinki, Finland
[3] Department of Physics and Astronomy, Division of Materials Theory, Uppsala University, PO Box 516, SE-751 20 Uppsala, Sweden
[4] Research Institute for Solid State Physics and Optics, Wigner Research Center for Physics, Budapest H-1525, Hungary
[5] Okmetic Oyj, PL 44, 01301 Vantaa, Finland

E-mail: ailaht@utu.fi

Received 19 December 2023; revised 20 May 2024
Accepted for publication 2 July 2024
Published 26 July 2024

CrossMark

Abstract
Polycrystalline silicon (poly-Si) significantly expands the properties of the ICT miracle material, silicon (Si). Depending on the grain size and shape and grain boundary structure, the properties of poly-Si exceed what single-crystal (c-Si) and amorphous (a-Si) silicon can offer, especially for radio frequency (RF) applications in microelectronics. Due to its wide range of applications and, on the one hand, its theoretically and technologically challenging microstructure, poly-Si research is the most timely (Ding *et al* 2020 *Mater. Charact.* **161** 110174; Zhao and Li 2019 *Acta Mater.* **168** 52–62). In this report, we describe

* Author to whom any correspondence should be addressed.

Original Content from this work may be used under the terms of the Creative Commons Attribution 4.0 licence. Any further distribution of this work must maintain attribution to the author(s) and the title of the work, journal citation and DOI.

© 2024 The Author(s). Published by IOP Publishing Ltd

how we simulate and analyse the phenomena and mechanisms that control the effect of poly-Si deposition parameters on the structure of the deposited poly-Si films using classical molecular dynamics simulations. The grain shape and size, degree of crystallinity, grain boundary structure and the stress of poly-Si films are determined depending on the growth temperature, temperature distribution in the growing film, deposition flux, flux variation and the energy transferred to the film surface due to the deposition flux. The main results include: (i) the dependence of the crystallinity profile of the deposited poly-Si films on the stress, temperature and the different parameters of the deposition flux, (ii) growth modes at the early stages of the deposition, (iii) interaction and stability of seed crystallites at the early stage of the deposition of poly-Si films and the transition from the isolated crystallite growth to the poly-Si growth, (iv) interplay of the temperature, crystallinity, crystal shape and heath conductivity of different Si phases, (v) four different stages of crystallite growth are described: nucleation, growth, disappearance and retardation.

Supplementary material for this article is available online

Keywords: polycrystalline silicon, deposition, computational materials physics, classical molecular dynamics

1. Introduction

Polycrystalline silicon (poly-Si) is an excellent functional material for microelectronics radio frequency (RF) applications to reduce their harmful electrical losses, nonlinearity and crosstalk. [1] Devices that contain Si/SiO_2 interface suffer from its inherent property of inducing a highly conductive layer at the Si surface close to the interface, called the parasitic surface conductive (PSC) effect (figure 1). Due to the PSC phenomenon, the resistivity of Si decreases, which can cause large currents, leading to harmful losses, non-linearity and crosstalk in RF applications. One way to prevent these harmful phenomena is to deposit a layer of poly-Si on top of Si. Then the mobile charge carriers induced by the PSC effect are trapped in the trap states existing in large amounts in the grain boundaries of poly-Si. [2–7]

The density of the trap states and their effectiveness in reducing loss, non-linearity and crosstalk depend on the detailed atomic structure of the grain boundaries, which in turn depends on the poly-Si growth parameters and post-treatments. [8] Starting from the growth parameters of poly-Si films, we investigate the structural properties of poly-Si grains and grain boundaries. For example, we solve the range and extent of the interaction between Si seed crystallites embedded in a-Si and how the thermal conductivity difference between c-Si and a-Si affects the growth of poly-Si. The information and data obtained pave the way for the design of poly-Si films for even more challenging applications. Besides RF-applications, poly-Si is used e.g. in solar cells, thin film transistors and waveguides of photonics circuits. Before presenting the details of our work, we briefly review some experimental and theoretical studies related to our research.

Using scanning electron microscope (SEM) Ogane [9] studied substrate preparation and grain size controlling of poly-Si films. He also studied surface structures of poly-Si using Kelvin force microscopy. Kočka *et al* [10] showed the transition from amorphous Si to microcrystalline and polycrystalline Si. In addition, Raman spectroscopy was used to evaluate the crystalline fraction; elastic recoil detection analysis as well as conductivity and photoconductivity measurements. Grazing incidence x-ray diffraction was used by

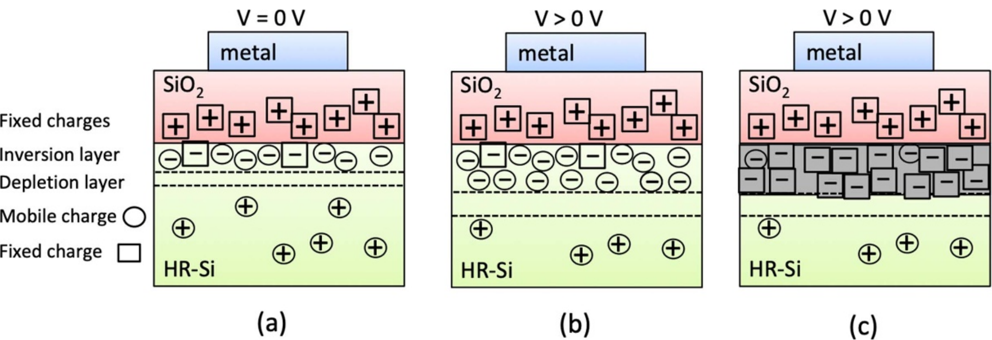

Figure 1. Illustration of the PSC in a metal-oxide-semiconductor device. (a) High resistive p-type Si (HR-Si) is oxidised and provided with a metal contact. At the Si-SiO_2 interface an inversion layer is induced. The mobile electrons in the inversion layer lead to PSC at the interface. (b) Positive bias even enhances this effect (negative bias induces accumulation of mobile holes, which in turn leads to PSC). High electrical conductivity causes many harmful phenomena in RF applications. (c) The detrimental effect of PSC can be mitigated by depositing a layer of poly-Si (grey) on top of the HR-Si. The charge carrier traps of poly-Si effectively reduces PSC.

Orapunt *et al* [11] to study amorphous-to-crystalline phase transition in Si-films. Raman spectroscopy was used to determine the crystalline volume fractions.

Keblinski *et al* [12] performed molecular-dynamics simulations using the Stillinger–Weber potential to synthesise nanocrystalline silicon by crystallisation from the melt. The obtained grain size was up to 7.3 nm. Grain boundaries were found to be similar to amorphous silicon. Molecular dynamics simulations of atom and cluster deposition of silicon has been studied by Biswas *et al* in 1988 [13] and by many others since [14–16]. Ohira *et al* [17] have investigated the growth process of silane-based chemical vapor deposition of microcrystalline silicon using molecular dynamics. Zhu *et al* [18] investigated the growth of coupled silicon grains under various growth velocities using the phase field method. Mei *et al* [19, 20] have developed a grain-growth model for poly-Si.

The rest of the paper is organised as follows. The simulation methods are presented in section II, where, for the sake of completeness, it is also explained how the values of the numerical parameters used in the simulations have been determined. In the third section, we analyse the deposition of poly-Si films with respect to external conditions like temperature, pressure and strain and internal conditions that play a role in the growth and quality of poly-Si films. Finally, we summarise our main findings from the simulation results, the physical cause-and-effect relationships involved in poly-Si fabrication, and the relationships between material properties and poly-Si deposition conditions.

In Part II [21], we study the structure of poly-Si films: distribution of the grain size, average thickness of grain boundaries, crystal orientation of the grains and distribution of 3-, 4-, and 5-coordinated atoms, i.e. properties that are directly related to the electrical properties of poly-Si.

2. Methods of simulation

The Large-scale Atomic/Molecular Massively Parallel Simulator (LAMMPS) molecular dynamics simulator [22] is used to investigate the fabrication of poly-Si films. Atomsk program

[23] is used to generate special atomic structures. For the visualisation and characterisation of the simulated structures OVITO visualisation tool [24] is used.

A typical simulation cell is a rectangular parallelepiped with a square base with sides from 6 to 10 nm and height from 20 to 30 nm (about 1 00 000–2 00 000 atoms). The largest simulation cell is $40 \times 40 \times 20\,\mathrm{nm}^3$ (about 10 00 000 atoms). At the sides of the simulation cell, periodic boundary conditions were used, whereas fixed boundary conditions were used at the bottom and the top of the cell.

The following eight different interatomic potentials were tested: Stillinger–Weber (SW) [25], Tersoff and two modified Tersoff [26–28], Edip [29], two meam/spline -potentials [30, 31] and snap-potential [32]. First, the following quantities were considered: lattice parameter, melting temperature and elastic constants. The calculated values were compared with the corresponding experimental data. Based on these four potentials (SW, Tersoff/mod, Tersoff/mod/c and Edip) were selected for further tests.

The epitaxial growth of single-crystal Si is the second test for the potentials. SW and Tersoff/mod lead quite similar crystalline growth, whereas Tersoff/mod/c produces amorphous Si. The Edip potential results are in between. Based on these tests, we chose SW potential for our polycrystalline Si investigations. The SW potential is widely used in Si studies. It provides a fairly good description of different defects [33], which are of relevance when dealing with grain boundaries. In addition, it is not very heavy computationally, which is a significant advantage when performing large-scale simulations.

While in the epitaxial growth simulations the substrate was single-crystal Si, we used poly-Si as the substrate in finding the optimal values of the computational parameters of the poly-Si deposition. Optimisation of the parameters is discussed in more detail in the supplementary material.

The flux of Si atoms (Φ) to the surface depends on the time between the successive Si atom additions to the system (Δt) and the surface area of the substrate (A), ($\Phi = 1/(\Delta t A)$). Typically in simulations fluxes Due to the limited sizes of simulation cells, we found differing results when applying the same flux to different surface areas. This necessitates separate consideration of the flux components. One of the figures of merit for the quality of the poly-Si films we use is the ratio of atoms in the crystalline phase to the total number of atoms. To reach about 90% diamond structure level in the deposited film the base area of the simulation cell should be at least about $40\,\mathrm{nm}^2$ and the time interval between the successive Si atom depositions should be at least about 300 fs. (Unless otherwise stated, the flux in this study is $\Phi \approx 8 \times 10^{-5} (\mathrm{nm}^2 \times \mathrm{fs})^{-1}$). The lower limits of Δt and A to obtain a good polycrystalline film can be understood because crystallisation mechanisms require a certain amount of time and space to complete before too many amorphous Si layers are deposited on the surface burying and locking the previously deposited deeper layers in a non-crystalline phase.

The ratio of the atoms in the crystalline phase to the total number of atoms in simulated poly-Si films was considered and the function $K_{A,\Delta t} = c_1/A + c_2/\Delta t + c_3$ was fitted to the data (at 900 K) obtained from the simulations. The crystallinity ratio is found to follow the formula (equation (1)) (more details in supplementary material).

$$K_{A,\Delta t}(A, \Delta t) = -\frac{315.3\,\mathrm{nm}^2}{A} - \frac{882.6\,\mathrm{fs}}{\Delta t} + 98.09 \quad [\%]\,. \tag{1}$$

An important technological parameter in film growing processes is the temperature of the substrate (T). We performed test simulations at different temperatures from 600 to 1400 K to find the suitable simulation temperature range for our chosen interatomic potential. The best polycrystalline growth (least amount of a-Si between the grains) is obtained approximately within the temperature range 900–1200 K.

During the deposition simulation, the surface temperature of the deposited film tends to rise due to the energy brought to the surface by the deposited atoms. Depending on the damping parameter of the thermostat in LAMMPS (τ), the speed of the deposited atoms and the time between the successive launches of the atoms (Δt) the final surface temperature of the poly-Si film in our simulations was 100–200 K higher than the temperature set to the thermostat. Toku *et al* [34] have studied experimentally the surface heating due to the deposition process of TiO_2 film. They report the surface to reach 50–80 K higher temperature compared to the bottom of the film. (Unless otherwise stated, temperature in this study refers to thermostat temperature.)

The speed of the atoms landing on the surface has a significant effect on the quality of the deposited poly-Si film. This was investigated by simulations at 900 K and using the initial speed of the atoms perpendicular to the substrate surface ($6 \times 6\,\mathrm{nm}^2$) from $0.1\,\mathrm{nm\,ps}^{-1}$ to $20\,\mathrm{nm\,ps}^{-1}$. If the time between successive Si atom additions Δt is short $\lesssim 100\,\mathrm{fs}$, no crystalline growth is observed or the crystallinity is poor. For these Δt, increasing the speed of deposited atoms does not significantly improve the quality of the poly-Si film. If $\Delta t \gtrsim 250\,\mathrm{fs}$, the quality of the poly-Si film improves with increasing speed of the deposited atoms up to about $10\,\mathrm{nm\,ps}^{-1}$. More information on the effects of computational parameters on Si deposition can be found in the supplementary material.

3. Simulations of the deposition of poly-Si films

The typical evolution of the poly-Si growth process during simulations is such that in the initial phase the growth continues as amorphous. Embryos of crystallites are then formed, some of which develop into Si crystallites. Eventually a poly-Si structure is formed. The transition from the growth type of a sparse network of small Si crystallites to the growth type of complete poly-Si occurs typically quite suddenly and simultaneously in the whole simulation cell. In figure 2 an example of the final grain structure is presented with each colour representing a grain (non-grain atoms have been removed for clarity).

Issues such as temperature distribution within the simulation cell, stress, stability of crystallites embedded in an amorphous substance and interactions between crystallites were investigated to further understand the formation of poly-Si layers. These topics are discussed in more detail in the following subsections.

3.1. Growth on amorphous Si substrates

In section 2 the simulation parameters were optimised using polycrystalline substrates enabling immediate poly-Si growth and saving the simulation time. The following depositions consider the growth of poly-Si starting from homogeneous substrates. In simulations, it is challenging to grow polycrystalline film starting from a perfect single-crystal substrate or a single-crystal with point defects. Using optimal simulation parameters leads to single-crystal growth, whereas if the simulation parameters were not well optimised crystalline growth was not obtained. However, if the substrate is a single-crystal covered by an amorphous film, polycrystalline growth is obtained.

In our simulations of the deposition of poly-Si films the substrate typically consists of a single-crystal slab ($10 \times 10 \times 1\,\mathrm{nm}^3$) with an amorphous Si layer ($10 \times 10 \times 1.5\,\mathrm{nm}^3$) on top. Usually, the surface of single-crystal wafers is amorphous after typical chemical treatments. Before the simulations, the substrate is relaxed by LAMMPS energy minimisation (except the 0.5 nm layer at the bottom of the cell). The thermostat in the simulations is set to 900 K. The velocity of the depositing Si atoms is $0.1\,\mathrm{nm\,ps}^{-1}$ towards the substrate. The direction of the

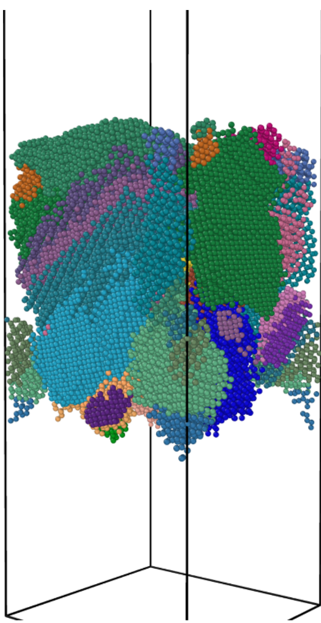

Figure 2. An example of a deposited poly-Si film. Each colour represents an individual grain (atoms in non crystalline phase have been removed). Note the simultaneous appearance of the tiny crystallites that grow into big grains. Crystallites were typically present also in the lower part as well, but they disappeared before reaching the critical size.

velocity of the depositing atoms is sightly randomised by selecting the velocity component parallel to the substrate surface randomly within the range (-0.005 nm ps^{-1}, 0.005 nm ps^{-1}), for both *x*- and *y*-directions. The total number of deposited Si atoms is 875 00, which leads to about 20 nm thick Si films.

Figure 3(a) is taken halfway through the simulation (about 10 nm thick deposited film). The simulation starts with amorphous (grey) growth with small crystalline (coloured) droplets. When about 10 nm film thickness is achieved, the first larger crystallites start to emerge. As the deposition continues, these larger crystallites grow and meet each other and a columnar growth mode begins forming a packed poly-Si layer (figure 3(c)). The simulation is stopped when the poly-Si layer is about 10 nm thick. Figure 3 shows four different stages of poly-Si film growth: (a) first crystallites are formed, (b) crystallites grow, (c) some crystallites meet and grain boundaries start to form, and (d) poly-Si film starts to form. The transition zone from the sparse crystallite phase to the poly-Si phase is about 3 nm thick. The interface between the amorphous phase and the poly-Si phase is quite sharp in 10×10 nm^2 and smaller simulation cells. In 40×40 nm^2 simulation cells, the interface between the amorphous phase and the poly-Si phase is rougher. Small Si crystallites interact with each other and increase each other's growth rate. However, the range of this interaction is short, only a few nanometers (see section 3.4.2). In larger simulation cells, the short-range interaction cannot accelerate the crystallite growth in the whole simulation cell simultaneously and the interface becomes rougher. The poly-Si film grows slowly also downwards due to the crystallisation of the amorphous Si.

The SEM investigations (figure 4) suggest that a similar kind of growth occurs also in commercial poly-Si fabrication processes; the growth starts with small crystallites which grow and

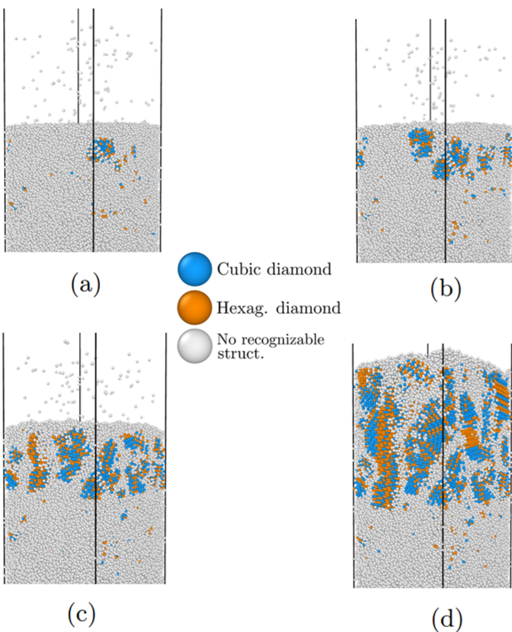

Figure 3. Snapshots of the growth of the poly-Si film. (a) First crystalline droplets form, (b) droplets grow and form crystallites, (c) crystallites continue to grow, meet each other and the grain boundaries start to form, and (d) continuous polycrystalline film is growing.

form a structure consisting of approximately parallel rods whose diameter increases towards the surface.

The effect of a short pause (0.2 ns) in the deposition process is shown in figure 5. During the pause, the crystallisation at the surface of the film continues producing larger grains than what would have been possible during the continuous flow of deposited atoms on the surface. When the deposition starts again the polycrystalline growth adapts to the larger crystals formed on the surface. This suggests one possible method to make interfaces and layers in poly-Si films. Ogane [9] has experimentally observed a similar phenomenon and explained that it is due to the increase in crystallite size during the deposition pause. However, the time scale in the experiments is orders of magnitude longer than in our simulations.

The post-annealing of the just-grown poly-Si film leads to a slight narrowing of the grain boundaries. This is due to the crystals growing slightly towards grain boundary regions (recrystallisation). As a result, the average size of the crystallites increases slightly.

3.2. Effect of growth temperature on the grain size

The previous simulations were repeated at 700 K and 800 K temperatures and from the resulting poly-Si films the crystallinity was analysed by using the OVITO program. Assuming equally sized grains and equal grain boundary thicknesses, the average grain size and boundary thickness is estimated based on the crystallinity fraction. The effect of temperature on these is shown in table 1. Increasing the growth temperature increases the average grain diameter and decreases the average thickness of the grain boundaries. Increasing the growth temperature from 700 K to 900 K has quite substantial effect on both quantities. Because the increase in

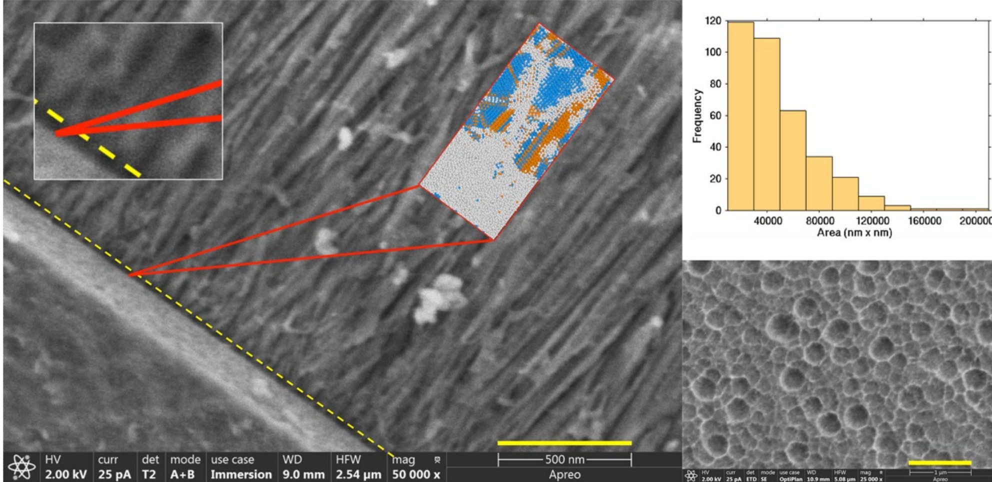

Figure 4. Left: a scanning electron microscope (SEM) image of the cross-section (side view) of a poly-Si film (above the light-grey step) deposited on a c-Si wafer (below the light-grey step), yellow bar shows 500 nm distance. The light-grey step is due to the sample preparation (the etch rate of poly-Si is higher than that of c-Si). SEM image (μm scale) can be compared with a typical simulation (red $\sim$25 nm long parallelepiped), the yellow dashed line separates an $\sim$25 nm thick initial layer of poly-Si (black). Above that line larger grains can be seen (different shades of grey, magnification in the upper left corner). Right, low: SEM image (top view of the same poly-Si wafer) the surface consists of rounded cross-sections of crystallites, yellow bar shows 1 μm distance. Right, up: distribution of the cross-sectional areas of the grains obtained from the surface SEM image.

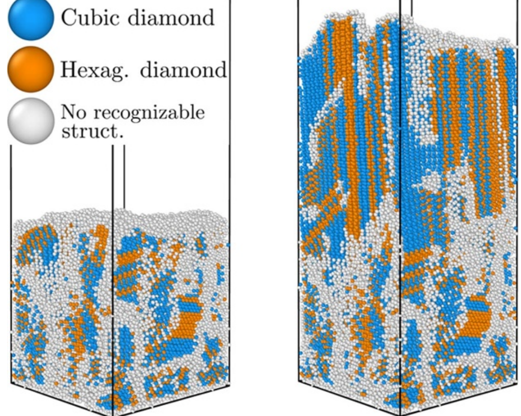

Figure 5. A distinct interface produced by a short break (0.2 ns) in Si deposition. Left side shows the structure during the break, right shows the resulting structure after we have continued the deposition. During the break the grain size in the surface increases, similar to post annealing. After the break the growth continues with a larger grain size.

Table 1. The effect of the growth temperature (T) on the average grain diameter (d_G) and the average thickness of the grain boundaries (d_{GB}), obtained from LAMMPS simulations.

T (K)	d_G (Å)	d_{GB} (Å)
700	23.1	5.6
800	23.8	5.1
900	30.2	4.3

average grain diameter is larger than the decrease in the average thickness of the grain boundaries it means that some of the smaller grains have disappeared.

3.3. Surface temperature

Deposited atoms bring energy to the surface, which raises the temperature at the surface. The key considerations here are: the number of deposited atoms per surface area per time unit, how quickly the simulation thermostat can react to the local temperature changes and how the temperature changes affect the poly-Si layer and its formation.

3.3.1. Temperature distribution in poly-Si during the deposition. To examine the temperature distributions in the deposited films during growth, a simulation cell is created with a starting substrate of roughly $7 \times 7 \times 2.5\,\text{nm}^3$ (two unit cells thick c-Si layer at the bottom, the rest a-Si). The atomic positions in the first few atomic layers (0.6 nm) are fixed. Silicon atoms are deposited towards the surface at the speed of $0.7\,\text{nm}\,\text{ps}^{-1}$ with five different deposit paces (time interval between the subsequent atoms (Δt)). The thermostat used in the simulation is the LAMMPS Nosé–Hoover style thermostat [35]. The thermostat is set to 900 K. When using LAMMPS, a key parameter of the thermostat is the damping parameter (damping (τ)) given in time units. A damping value of 100 fs would mean that the thermostat attempts to relax the temperature roughly in 100 fs. We test the effect of the damping parameter first. After an initial scan for the suitable range, five damping values are chosen for testing.

For the temperature distribution analysis, the simulation cell is vertically divided into 1 nm thick blocks (≈2500 atoms per block) and the temperature is calculated for each block, which gives us the vertical temperature distribution in the simulation cell. The temperature is found to be close to the thermostat values at the bottom of the cell. The temperature increases fairly linearly as a function of the height of the poly-Si film. How much the surface temperature is higher than the thermostat temperature depends on the rate of atoms coming to the surface. Once the deposition ends, the temperature differences in the cell become smaller and the whole system relaxes to the thermostat temperature at a rate determined by the thermostat damping parameter.

With five deposition rates and five damping values, we get a total of 25 simulations whose temperatures can be analysed. The average temperatures of the topmost (fully deposited) temperature calculation block are shown in figure 6. Two extreme cases (according to the crystallinity percentage) of these depositions are presented in figure 7. In the left side case, the deposition pace of atoms is higher, leading to higher surface temperatures and the poly layer starting to form earlier. The resulting poly-Si film contains only a few large grains. In the right side case, the average temperature at the surface is nearly a 100 K lower and consequently the poly-Si layer can be seen to start later and consist of many small grains.

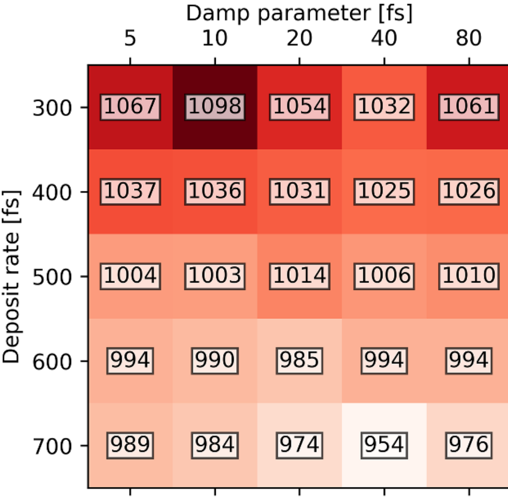

Figure 6. Temperature at the surface (average temperature in the 1 nm thick surface layer) with different deposit paces and damping values of the thermostat.

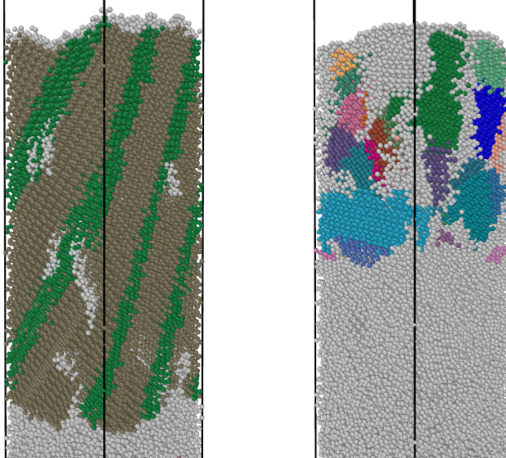

Figure 7. Grain structure after deposition with 300 fs deposit interval and 40 fs damping parameter (left) and with 700 fs deposit interval and 20 fs damping parameter (right). In the case on the right, the average surface temperature is almost a 100 K lower than on the left. Atoms in the figure are colored based on the grain they belong to.

The effect of the damping parameter on the surface temperature is not as clear as the effect of the deposition interval. However, a damping value of 40 fs seems to regulate the temperatures best (compared to the thermostat value of 900 K) (figure 6). With this limited data, the effect of damping on the structure of the poly-Si layer appears to be more coincidental than observable.

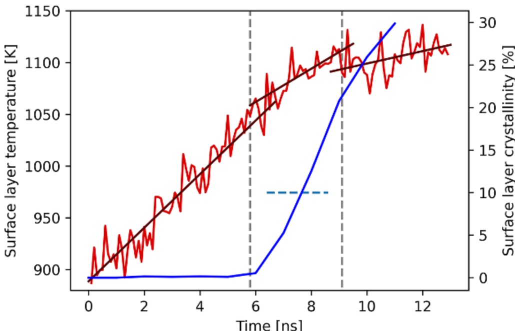

Figure 8. Surface temperature (average temperature in the 2 nm thick surface slice) as a function of deposition time in red (left vertical axis) and the portion of atoms within the surface slice that are in the crystalline structure in blue (right vertical axis). The criterion of the threshold for the start of the polycrystalline growth is marked with the blue horizontal dashed line. The vertical dashed line at about 6 ns marks the beginning of the exponential growth of crystalline phase and the vertical dashed line at about 9 ns marks its end.

3.3.2. Temperature and crystallinity at the growth front during depositions. We further analyse the simulation data to obtain more detailed information about the internal state of the growing poly-Si films. Surface temperatures and percentages of atoms in the crystalline structure near the surface are monitored as a function of the deposition time. Figure 8 shows the temperature (red) and the proportion of crystalline Si (blue) in the topmost 2 nm thick surface slice of the deposited film as a function of deposition time. The deposit pace was chosen to be 400 fs and the damping parameter was 40 fs. We are interested in the height (thickness) of the film and the surface temperature of the film just at the region where the amorphous layer at the surface transforms to poly-Si (critical height and temperature). In this context, we consider the start of the polylayer when the degree of crystallinity exceeds 10% at the topmost 2 nm. At this threshold, the bottom part of the analysed 2 nm block is still amorphous but crystallite seeds have formed at the top of block, which based on manual visual analysis develop to the polysilicon structure in each of our cases. This threshold crystallinity is indicated in figure 8 by a blue horizontal dashed line.

This kind of analysis was done for all previously discussed 25 simulations. The critical film height (at the moment the poly-Si starts to form) and the critical surface temperature averages are shown in figure 9. The surface temperature and the film height are inversely proportional. Doubling the deposition pace halves the height where the poly-Si starts to form. The halved height and doubled deposition speed mean that it takes only a quarter of the simulation time for the poly-Si to start to form with the higher deposition interval (estimated from figure 9).

A more detailed analysis of figure 8 reveals new features of poly-Si deposition and provides useful atomic-level information on the crystallisation of poly-Si films. Crystallisation in the 2 nm thick surface slice of the poly-Si film was monitored for 13 ns. During the first nanosecond, the first crystallite cores develop. The rates of creation and disappearance of crystallite cores balance each other (the volume of crystalline Si is constant) up to 6 ns from the beginning of the deposition. At that point, the temperature of the surface slice has risen to about 1000 K and the rapid three-dimensional growth of the crystallites begins. This can be seen as an exponential increase in the total volume of crystalline Si in the surface slice. This 3-dimensional growth continues for about 3 ns. After that, the crystallites in the surface slice start to touch each other, poly-Si is formed and the grain growth becomes 1-dimensional towards the open

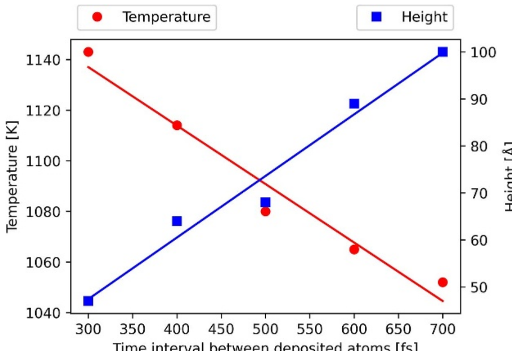

Figure 9. Temperature of the 2 nm thick surface slice when the poly-Si starts to form as a function of deposition interval (left vertical axis) presented in red with circles. Position (height) of the surface slice from the bottom of the simulation cell when the poly-Si starts forming (right vertical axis) presented in blue with squares.

surface of the growing film. This can be seen as the termination of the exponential growth of the volume of the crystalline part in the surface slice.

3.3.3. Rate of heating. In the surface slice, taking into account the rate of temperature rise, three different regions are clearly distinguished, just like in the crystallinity. During the first 6 ns, the temperature rises by about 25 K ns^{-1}, which then drops to about 17 K ns^{-1} at 6 ns. At about 9 ns the temperature rise drops to 7 K ns^{-1}. These three temperature sections can be related to the heat conduction of different phases of Si. According to experiments, the thermal conductivity of a-Si is about 100 times lower than that of c-Si, and for poly-Si, it is between those of a-Si and c-Si [36–38]. During the first 6 ns, the surface slice consists mainly of a-Si, whose thermal conductivity is low leading to slow dissipation of the thermal energy brought to the surface by the deposited atoms. Therefore, the temperature rise at the surfasc is fast. When larger crystallites start to form at 6 ns, the average thermal conductivity increases leading to a slower increase in the temperature of the surface slice. At 9 ns, such crystalline grains begin to form that extend almost through the surface slice. That increases the thermal conductivity further, leading to a significantly slower temperature rise at the surface slice. These three distinct temperature rise phases were also observed in other simulations.

3.4. The nucleation and growth of the seed cores of the Si crystallites

The stability of the seed cores of crystallites in a crystallising amorphous medium depends on the size of the crystallite cores. There is a threshold size below which the crystallite core tends to disappear and above which it tends to grow (a collection of simulated newly born primary crystalline Si cores can be seen in figure 3) [39, 40]. We investigated the stability of isolated crystalline Si cores in amorphous Si using our simulation setup: LAMMPS, SW potential and Nosé–Hoover thermostat. We can then compare these with the predictions from classical nucleation theory [41]. The possible mutual effect of two neighbouring crystalline Si cores on their stability and growth was also investigated.

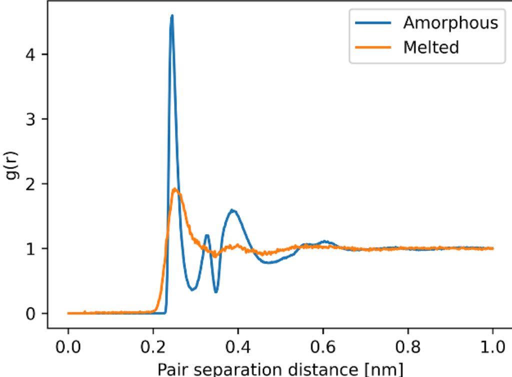

Figure 10. Radial distribution function ($g(r)$) of the melted silicon and the amorphous end result.

3.4.1. Single-crystal Si cores in an amorphous Si medium. To study the stability of the c-Si cores, an amorphous Si block is first constructed. This is done by a melt-cooling process. Single-crystal Si block is melted at 3000 K and cooled down at the rate of 10^{12} K s^{-1}. Radial distribution functions for the melted Si and the amorphous Si are shown in figure 10. The obtained radial distribution function of amorphous Si compares well with that by Fusco *et al* [42].

From the prepared amorphous Si block, the atoms can then be removed from a sphere of a certain radius and replaced by a sphere cut similarly from a single-crystal Si block. The total number of atoms is ensured to remain the same in this substitution. The obtained Si block is then relaxed with LAMMPS energy minimisation. Finally, these amorphous Si blocks with a c-Si core at the centre were set to a temperature of 900 K (similar temperatures as used in the growth simulations) and simulated to examine the evolution of the crystalline cores. Different radii are tested with individual Si cores as well as Si core pairs with different separation distances.

At different points in the simulations, we used a method based on the atomic energy [40] to determine the radius of the c-Si core, see figure 11. The average energy per atom as a function of the radial distance from the centre of the c-Si core is calculated. The curve has two plateaus, the amorphous phase at the higher energies and the crystalline phase at some 0.3 eV lower energy. A sigmoid function is fitted to the energy values and the position of the midpoint value of the sigmoid curve is taken to be the radius.

The simulations are performed in a cubic cell of amorphous Si with a side length of 15 nm. The investigated c-Si cores had radii 0.8, 1, 1.2, 1.4, 1.6 and 1.8 nm. For each radius, seven different simulations are performed (for better statistics). The radius development during the simulation is shown in figure 12, where the radius of the Si core is plotted as a function of the simulation time. The curve shows the averaged values from the seven simulations per initial radii. The Si cores that disappeared during the simulation are not counted at this point. Such Si cores were found at the three smallest initial radii (0.8 nm, 1 nm and 1.2 nm). Test cases with smaller radii all disappeared. Classical nucleation theory, based on the values found in the work of Spinella *et al* [41], estimates the critical radius to be about 0.6 nm which aligns with our observations.

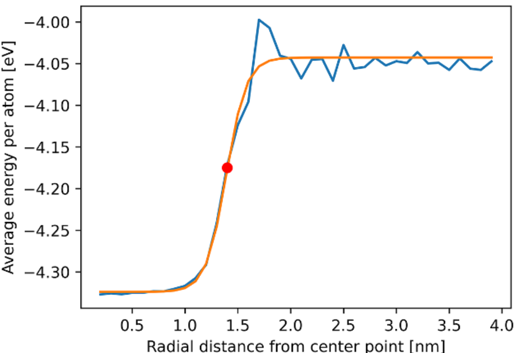

Figure 11. Radial average energy per atom as a function of the distance from the centre of a c-Si core and a sigmoid function fitted to the energy values. Midpoint (red mark) is used for radius determination.

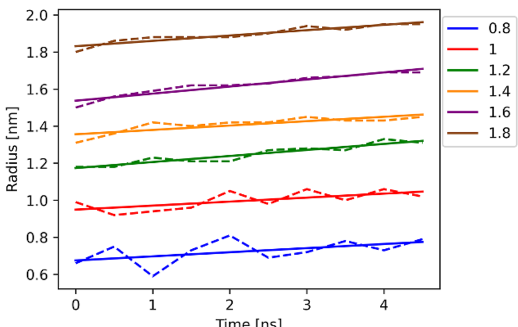

Figure 12. Radius of the Si core during the simulation averaged from the seven simulations for each initial radius. Cases where the Si core disappeared during the simulation have been removed from the averaging. Initial radii (cut-radii from the crystalline Si) in the legend are given in nm. The slopes of the fitted lines at the different radii can be found in figure 13. The curves do not start exactly at the radii shown in the legend because the Si cores are first relaxed in amorphous Si and then the radii are obtained using the method as shown in figure 11.

Lines have been fitted to the curves and the slope is used to compare the growth rates of the Si cores. The average slopes for the unstable (0.8 and 1.0 nm), semi-stable (1.2 and 1.4 nm) and stable (1.6 and 1.8 nm) starting radii are shown in figure 13.

Disappearing/non-growing Si cores were found only at the three smallest starting radii. To highlight the instability of the Si cores with smaller initial radii, the deviation from the average radius is calculated for each simulation and shown in figure 14. The larger radii produce quite predictable results of growth leading to small deviations. At the smaller radii some simulations exhibit very low to negative growth rates (some outright disappearing) with only few exhibiting comparable positive growth than those of larger initial radii. Possibilities of outcomes therefore are more varied, which lead to the higher deviations found in figure 14.

As c-Si cores grow, their centre moves due to randomly different growth rates on different sides of the Si cores. To analyse this movement of the Si cores, the centre points are determined both at the beginning and at the end. This was done by identifying the Si core with the Ovito Polyhedral template matching structure identification algorithm, selecting the atomic positions

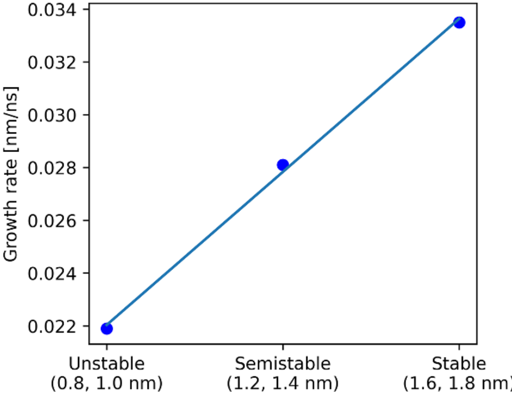

Figure 13. The results in figure 12 have been classified into three groups: unstable ones with the smallest starting radii, stable for the largest starting radii and semi-stable for the in-between ones. Average growth rates for the three are calculated from the slopes of the linear fits in figure 12.

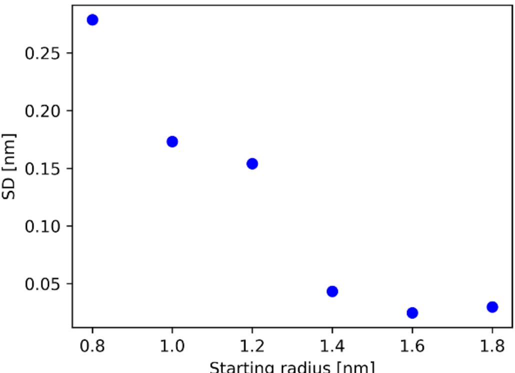

Figure 14. Standard deviation of the Si core radii at the end of the different simulations as a function of different starting radii.

in the Si core and calculating the centre point of the atomic positions. The average shift of the centre point determined from five simulations per starting radius are from 0.2 to 0.4 nm during 5 ns simulations at the thermostat temperature of 900 K. The calculated displacements were mostly within a few tenths of nanometers, except for a few larger deviations, the largest of which is 0.7 nm. The determination of the centres of the c-Si cores does not account for the shape change so the centre point shift can be also due to the change in the shape rather than the movement of the Si core.

3.4.2. Interaction between crystalline Si cores. To test whether neighbouring c-Si cores have an impact (mediated by atoms in between) on each other, two Si cores were placed in an amorphous cell large enough to minimise the effects of the periodicity (Si core interacting with its periodic counterpart). The distance between the Si cores is varied and their time development at the 900 K temperature is analysed. The Si cores are initially spheres with an initial radius of 1 nm and edge-to-edge separation distances of 0.5, 0.75, 1.0, 1.25, 1.5, 2.0, 2.25 and

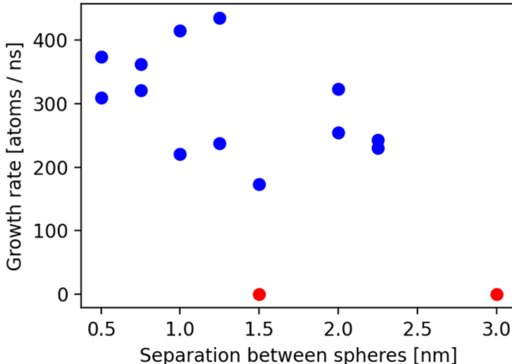

Figure 15. Growth rate of the crystalline Si cores in the presence of a nearby Si core as a function of the distance between the Si cores.

3.0 nm are investigated. The increase in the number of crystalline atoms per ps (growth rate) with the different separation distances are shown in figure 15. The marks shown are the growth rates of individual Si cores (two per simulation cell) with the points marked with red being ones where the Si core disappeared during the simulation (one at 1.5 nm, both at 3.0 nm).

These simulations suggest that nearby c-Si cores aid each other in growing. The highest growth rates are seen with the shortest distance whereas at the largest distance both Si cores disappeared. This type of phenomenon can lead to the explosive-like formation of a polycrystalline phase when the density of crystalline cores has reached a critical level. The statistical nature of the growth process and the limited amount of data somewhat limit the conclusions that can be drawn from our Si core simulations. The results obtained here are in line with our growth simulations where in all base area $10 \times 10\,\mathrm{nm}^2$ cases the transition from the isolated crystallite phase to the poly-Si phase is very sharp and occurs at the same level and time in the whole simulation cell (see figure 3).

The phenomena related to the c-Si cores studied here could have a connection to the directionality of the interatomic interactions. For instance, Fusco *et al* [42] state that there is a connection between local plastic activity and coordination defects in amorphous systems depending on the nature of the interatomic interactions. In particular, the directionality of the bonds, as quantified by the three-body term in Stillinger–Weber-like interactions affects not only the role of local defects, but also the size of the plastic rearrangements, and the global stress–strain behaviour.

3.5. Effect of pressure and material stress on poly-Si growth

3.5.1. Pressure. In the fixed pressure simulations, due to the free surface of the film, the simulation cell does not change in the vertical direction. In the lateral direction, the cell expands about 4‰–6‰. This is so small change that it does not have discernible effects on the produced poly-Si film. The statistical variation between different simulations produces typically larger effects than the 4‰–6‰ lateral expansion.

3.5.2. Stress in the simulation box. One possible key to increasing understanding of the growth process is to look at stress inside the simulation cell. To analyse this, we calculated the stress per atom within the cell. LAMMPS outputs the stress tensor for each atom. To visualise

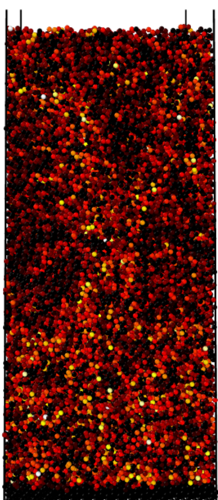
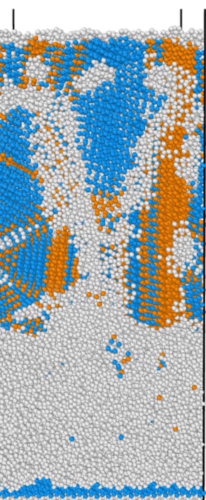

Figure 16. A poly-Si film analysed according to stress (left) and structure (right). On the left is the colormap of per atom stresses with darker colours representing lower stress and brighter colour higher stress. On the right is the structure identification of the same simulation (blue for cubic diamond, orange for hexagonal diamond and white for amorphous).

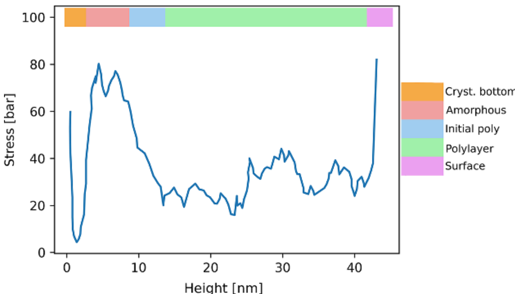

Figure 17. Stress as a function of the height (within the deposited film) with the different regions highlighted from the starting base with the crystalline part to amorphous layer, the transition region, the proper poly layer and the surface layer.

the stress, the data eigenvalues are solved for the stress tensor to get the principal stresses and the largest of these is taken and shown with the colour mapped simulation box shown on the left in figure 16. Average stress as a function of the height of the poly-Si layer is calculated and shown in figure 17.

If we compare these with the structure identification data (on the right in figure 16) we see that stresses mostly show similar information with higher stress areas corresponding with amorphous, grain boundaries and other non-ordered regions and lower stress areas correspond with crystalline areas.

4. Conclusions

We have studied crystallization in the fabrication of polycrystalline silicon (poly-Si) films using the LAMMPS molecular dynamics package [22]. The interaction between atoms was modeled with the Stillinger–Weber potential [25]. The largest simulation cells used contain about 10 00 000 atoms. The investigated phenomena range from the Ångström scale to the 0.1 μm scale.

Depositing Si on substrates with crystalline Si on the bottom and an amorphous Si (a-Si) film on top, the deposition starts in amorphous form. Depending on the values of the deposition parameters, after a certain time, the amorphous growth first changes to the form of crystalline pockets in a-Si and later to the polycrystalline form, continuing in the mode of increasing grain size. At least part of the increasing average grain size can be related to the increasing surface temperature during deposition. Features of the sudden onset of the poly-Si formation and the gradual increase of the grain size as a function of poly-Si film thickness were observed also in larger scales in SEM studies.

A short total break of the deposition caused a clear interface in the poly-Si film due to an increase in grain size at the surface during the break. When the growth starts again, the produced average grain size is larger than before the break. According to the simulations, raising the deposition temperature increases the crystallinity of the poly-Si film up to 1120 K, after which the crystallinity starts to decrease. The higher crystallinity is mainly due to the increase in the average grain size. The thickness of the grain boundaries is decreased as well. Post-annealing of the just grown poly-Si film slightly reduces the thickness of the grain boundaries.

A typical deposition of poly-Si in a nanosecond scale proceeds as follows. During the first nanosecond, the first crystallite cores develop but the rates of their creation and disappearance balance each other up to 6 ns. At that point, rapid three-dimensional growth of the crystallites begins producing exponential increase in the total volume of crystalline Si. This 3-dimensional growth continues for about 3 ns. After that, the crystallites start to touch each other and the grain growth becomes 1-dimensional towards the open surface of the growing film. The three different observed phases of crystallinity can be related to the three different rates of the increasing surface temperature during the deposition, which in turn is related to the different heat conduction of a-Si and poly-Si.

Studying the seed nuclei of Si crystallites shows that there is a threshold size of the nuclei beyond which most of them continue to grow rather than decay. This threshold radius of the nuclei is estimated to be 1.2–1.4 nm. Si cores also have a clear impact on each other. Placing two crystalline Si cores in an a-Si cell and increasing their distance gradually suggests that their growth rate at a distance of 0.5 nm is twice the growth rate at a 5 nm distance. This kind of interaction can explain the explosive-like formation of a polycrystalline phase observed in the simulations.

No discernible differences were obtained in poly-Si growth using fixed volume or fixed pressure in the simulations. In fixed pressure depositions, the lateral dimensions of the unit cell changed only 4‰–6‰. Calculating the stress per atom within the simulation cell shows that amorphous-like grain boundaries possess higher stress than the crystalline grains.

Since the electrical properties of poly-Si are strongly dependent on their structure, the structural data and its relation to the growth parameters of poly-Si films provides useful information for future research on the electrical properties of poly-Si films.

Data availability statement

The data cannot be made publicly available upon publication because no suitable repository exists for hosting data in this field of study. The data that support the findings of this study are available upon reasonable request from the authors.

Acknowledgments

This work has been supported by Business Finland (Project BEETLES TY 1320731/2021) and Okmetic Oy. The computer resources of the Finnish IT Center for Science (CSC) and the Finnish Computing Competence Infrastructure (FCCI) Project (Finland) are acknowledged.

ORCID iDs

Mikael Santonen https://orcid.org/0009-0003-4633-4743
Antti Lahti https://orcid.org/0000-0001-7037-4946
Zahra Jahanshah Rad https://orcid.org/0000-0001-6943-2256
Mikko Miettinen https://orcid.org/0000-0002-5923-6507
Juha-Pekka Lehtiö https://orcid.org/0000-0002-4762-8554
Pekka Laukkanen https://orcid.org/0000-0003-4220-985X
Marko Punkkinen https://orcid.org/0000-0003-4952-0616
Petriina Paturi https://orcid.org/0000-0002-6240-2801
Kalevi Kokko https://orcid.org/0000-0002-4039-2745
Antti Kuronen https://orcid.org/0000-0003-0795-8003
Levente Vitos https://orcid.org/0000-0003-2832-3293

References

[1] Rack M, Allibert F and Raskin J-P 2021 Modeling of semiconductor substrates for RF applications: part II—parameter impact on harmonic distortion *IEEE Trans. Electron Devices* **68** 4606–13
[2] Cheng S, Chang Y-W, Gao N, Dong Y-M, Fei L, Wei X and Wang X 2017 Radio-frequency characteristics of partial dielectric removal HR-SOI and TR-SOI substrates *Chin. Phys. Lett.* **34** 1–5
[3] Amit I, Englander D, Horvitz D, Sasson Y and Rosenwaks Y 2014 Density and energy distribution of interface states in the grain boundaries of polysilicon nanowire *Nano Lett.* **14** 6190–4
[4] Mueller T, Johlin E and Grossman J C 2014 Origins of hole traps in hydrogenated nanocrystalline and amorphous silicon revealed through machine learning *Phys. Rev.* B **89** 1–7
[5] Ikeda H 2002 Evaluation of grain boundary trap states in polycrystalline-silicon thin-film transistors by mobility and capacitance measurements *J. Appl. Phys.* **91** 4637–45
[6] Kitahara Y, Toriyama S and Sano N 2003 A new grain boundary model for drift-diffusion device simulations in polycrystalline silicon thin-film transistors *Jpn. J. Appl. Phys.* **42** L634–6
[7] Ayres J R 1993 Characterization of trapping states in polycrystalline-silicon thin film transistors by deep level transient spectroscopy *J. Appl. Phys.* **74** 1787–92
[8] Schultz P A 2006 Theory of defect levels and the "band gap problem" in silicon *Phys. Rev. Lett.* **96** 246401
[9] Ogane A 2009 Polycrystalline silicon thin films with improved crystallographic and electronic properties for photovoltaic applications *PhD Thesis* Nara Institute of Science and Technology, Graduate School of Materials Science, Microelectronic Device Science Laboratory
[10] Kočka J *et al* 2004 The physics and technological aspects of the transition from amorphous to microcrystalline and polycrystalline silicon *Phys. Status Solidi* c **1** 1097–114
[11] Orapunt F, Tay L L, Lockwood D J, Baribeau J M, Noël M, Zwinkels J C and O'Leary S K 2016 An amorphous-to-crystalline phase transition within thin silicon films grown by ultra-high-vacuum evaporation and its impact on the optical response *J. Appl. Phys.* **119** 065702

[12] Keblinski P, Phillpot S R, Wolf D and Gleiter H 1997 Amorphous structure of grain boundaries and grain junctions in nanocrystalline silicon by molecular-dynamics simulation *Acta Mater.* **45** 987–98
[13] Biswas R, Grest G S and Soukoulis C M 1988 Molecular-dynamics simulation of cluster and atom deposition on silicon (111) *Phys. Rev.* B **38** 8154–62
[14] Xie J, Feng J and Lu H 1999 Molecular-dynamics simulation of low-temperature growth of silicon films by cluster deposition *Modelling Simul. Mater. Sci. Eng.* **7** 289–95
[15] Mazzone A 2002 Molecular dynamics simulations of impact of energetic silicon clusters onto crystalline silicon *J. Comput.-Aided Mater. Des.* **9** 1–9
[16] Ning N, Rinaldi S M and Vach H 2009 An atomic-scale study of hydrogenated silicon cluster deposition on a crystalline silicon surface *Thin Solid Films* **517** 6234–8
[17] Ohira T, Ukai O and Noda M 2000 Fundamental processes of microcrystalline silicon film growth: a molecular dynamics study *Surf. Sci.* **458** 216–28
[18] Zhu C, Koizumi Y and Guo C 2022 Grain boundary development of silicon during directional solidification: a phase-field study (arXiv:2206.04895)
[19] Mei L, Rivier M, Kwark Y, Dutton R W and Laboratories S E 1982 Grain-growth mechanisms in polysilicon *J. Electrochem. Soc.* **129** 1791–5
[20] Mei L and Dutton R W 1982 A process simulation model for multilayer structures involving polycrystalline silicon *IEEE Trans. Electron Devices* **29** 1726–34
[21] Lahti A *et al* 2024 Polycrystalline silicon, a molecular dynamics study: part II—Grains, grain boundaries and their structure *Modelling Simul. Mater. Sci. Eng.* **6** 065026
[22] Thompson A P *et al* 2022 LAMMPS—a flexible simulation tool for particle-based materials modeling at the atomic, meso and continuum scales *Comput. Phys. Commun.* **271** 108171
[23] Hirel P 2015 Atomsk: a tool for manipulating and converting atomic data files *Comput. Phys. Commun.* **197** 212–9
[24] Stukowski A 2010 Visualization and analysis of atomistic simulation data with OVITO-the open visualization tool *Modelling Simul. Mater. Sci. Eng.* **18** 015012
[25] Weber T A and Stillinger F H 1985 Local order and structural transitions in amorphous metal-metalloid alloys *Phys. Rev.* B **31** 1954
[26] Tersoff J 1988 New empirical approach for the structure and energy of covalent systems *Phys. Rev.* B **37** 6991–7000
[27] Kumagai T, Izumi S, Hara S and Sakai S 2007 Development of bond-order potentials that can reproduce the elastic constants and melting point of silicon for classical molecular dynamics simulation *Comput. Mater. Sci.* **39** 457–64
[28] Pun G P and Mishin Y 2017 Optimized interatomic potential for silicon and its application to thermal stability of silicene *Phys. Rev.* B **95** 1–21
[29] Justo J F, Bazant M Z, Kaxiras E, Bulatov V V and Yip S 1998 Interatomic potential for silicon defects and disordered phases *Phys. Rev.* B **58** 2539–50
[30] Lenosky T J, Sadigh B, Alonso E, Bulatov V V, Diaz De La Rubia T, Kim J, Voter A F and Kress J D 2000 Highly optimized empirical potential model of silicon *Modelling Simul. Mater. Sci. Eng.* **8** 825–41
[31] Du Y A, Lenosky T J, Hennig R G, Goedecker S and Wilkins J W 2011 Energy landscape of silicon tetra-interstitials using an optimized classical potential *Phys. Status Solidi* b **248** 2050–5
[32] Zuo Y *et al* 2020 Performance and cost assessment of machine learning interatomic potentials *J. Phys. Chem* A **124** 731–45
[33] Balamane H, Halicioglu T and Tiller W A 1992 Comparative study of silicon empirical interatomic potentials *Phys. Rev.* B **46** 2250–79
[34] Toku H, Pessoa R S, Liberato T B, Massi M, Maciel H S and Da Silva Sobrinho A S 2019 Effect of the substrate heating due to the sputtering process on the crystallinity of TiO2 thin films *ECS Trans.* **9** 189–97
[35] Shinoda W, Shiga M and Mikami M 2004 Rapid estimation of elastic constants by molecular dynamics simulation under constant stress *Phys. Rev.* B **69** 134103
[36] Wada H and Kamijoh T 1996 Thermal conductivity of amorphous silicon thin films *Jpn. J. Appl. Phys.* **35** L648–50
[37] Uma S, McConnell A D, Asheghi M, Kurabayashi K and Goodson K E 2001 Temperature-dependent thermal conductivity of undoped polycrystalline silicon layers *Int. J. Thermophys.* **22** 605–16

[38] Shanks H R, Maycock P D, Sidles P H and Danielson G C 1963 Thermal conductivity of silicon from 300 to 1400 K *Phys. Rev.* **130** 1743–8
[39] Von Alfthan S, Sutton A P, Kuronen A and Kaski K 2005 Stability and crystallization of amorphous clusters in crystalline Si *J. Phys.: Condens. Matter* **17** 4263–70
[40] Bording J K and Taftø J 2000 Molecular-dynamics simulation of growth of nanocrystals in an amorphous matrix *Phys. Rev.* B **62** 8098–103
[41] Spinella C, Lombardo S and Priolo F 1998 Crystal grain nucleation in amorphous silicon *J. Appl. Phys.* **84** 5383–414
[42] Fusco C, Albaret T and Tanguy A 2010 Role of local order in the small-scale plasticity of model amorphous materials *Phys. Rev.* E **82** 1–11
[43] Ding L, Raskin J-P, Lumbeeck G, Schryvers D and Idrissi H 2020 TEM investigation of the role of the polycrystalline-silicon film/substrate interface in high quality radio frequency silicon substrates *Mater. Charact.* **161** 110174
[44] Zhao D and Li Y 2019 Revealing the factors influencing grain boundary segregation of P, As in Si: insights from first-principles *Acta Mater.* **168** 52–62